JMEPEG (2013) 22:3034–3042
DOI: 10.1007/s11665-013-0605-0

1059-9495/$19.00

Microstructures and Properties of Friction Freeform Fabricated Borated Stainless Steel

J.J.S. Dilip and G.D. Janaki Ram

(Submitted March 26, 2013; in revised form May 19, 2013; published online June 1, 2013)

A new additive manufacturing process, termed "friction freeform fabrication," has been recently proposed by the authors. One of the unique capabilities of the process is that it can facilitate fabrication of three-dimensional parts in materials that are difficult to fusion deposit. The current study is a striking demonstration of this, in which cylindrical samples of 40 mm height and 10 mm diameter were successfully produced in borated stainless steel ASTM 304B4, a material known to be very difficult to fusion weld or deposit. Microstructures and mechanical properties of these samples were investigated in detail and were compared to those of standard wrought-processed alloy 304B4 Grade B material.

Keywords additive manufacturing, borated stainless steel, friction deposition, friction freeform fabrication, friction surfacing

1. Introduction

Additive manufacturing processes such as selective laser melting (Ref 1), electron beam melting (Ref 2), laser-engineered net shaping (Ref 3), and direct laser forming (Ref 4) work well for part fabrication in materials that are amenable for fusion deposition. However, these processes are at a disadvantage when dealing with materials that are susceptible to solidification cracking or liquation cracking. Further, in some materials, as the part is built layer-by-layer, cracking can occur in solid state because of a combination of brittle microstructure and residual stresses. It is, therefore, highly preferable to employ solid-state processes for additive manufacturing. Accordingly, the present authors have recently proposed a new additive manufacturing process, in which the build material is deposited in solid state by frictional heating (Ref 5, 6).

While it is possible to utilize "friction deposition" for additive manufacturing in several ways, the simplest of them involves the following (Fig. 1), which can be performed on a machine tool similar to a standard direct-drive rotary friction welding machine with necessary machining accessories. The build material is taken in the form of a rod (consumable rod) and is firmly held in the machine spindle. On the stationary side of the machine, a rod of slightly larger diameter than the consumable rod is placed, which serves as the substrate. The spindle is driven to a certain constant speed, and the two work pieces are brought together under a certain axial force (friction force). As the mating surfaces rub together, a layer of plastic material develops at the tip of the consumable rod because of frictional heating. When this layer attains the desired thickness, the process is terminated, by applying brakes on the rotating spindle and immediately moving the substrate away. The result is a circular layer of material deposited onto the substrate, diameter of which is slightly larger than that of the consumable rod. The layer is then machined to its slice contour. The layer is also surface machined to present a flat and even surface without any oxide scales for depositing the next layer. Similarly, the flash at the tip of the consumable rod is removed. The next layer is then deposited and machined. These deposition and machining steps are repeated until the entire part is built layer-by-layer. More details on the process and how it can be utilized for additive manufacturing are presented elsewhere (Ref 5). It should be noted that the process of friction deposition described above is, in principle, similar to friction surfacing, a well-known solid-state surface-coating process (Ref 7). Thus, the thermomechanical phenomena involved in friction deposition can be expected to be essentially the same as those involved in friction surfacing.

Borated stainless steels have originally been developed for neutron shielding purposes in nuclear industry. Essentially, they are austenitic stainless steels with significant additions of boron. ASTM Standard A887 covers eight different types of borated stainless steels, depending on the boron contents, ranging from 0.2 to 2.25% (Ref 8). For each type, the specification describes two grades—Grade A and Grade B. Materials processed to Grade A requirements (often via powder metallurgy route) contain significantly finer borides and uniformly distributed borides when compared with Grade B materials (normally produced using ingot metallurgy route). Consequently, Grade A materials show better tensile ductility and impact strength compared with Grade B materials.

With additive manufacturing processes involving fusion deposition, if parts can be successfully realized is largely determined by the fusion weldability of the build material. Weld fusion zones in borated stainless steels typically show a continuous interdendritic network of brittle boride + austenite eutectic, as can be seen in Fig. 2. Because of this, they exhibit very poor ductility and toughness (Ref 9, 10). Satisfactory weld ductility can only be achieved after a long, high-temperature

J.J.S. Dilip and **G.D. Janaki Ram**, Materials Joining Laboratory, Department of Metallurgical and Materials Engineering, Indian Institute of Technology Madras, Chennai 600 036, India. Contact e-mail: jram@iitm.ac.in.

post-weld heat treatment, which helps the boride eutectic to spheroidize and/or discretize, as reported by Park et al. (Ref 11). Further, borated stainless steels are susceptible to solidification cracking (because of their wide solidification range, as can be seen in Fig. 3) as well as liquation cracking in the partially melted zone (Ref 9, 10). These factors make borated stainless steels unsuitable for additive part fabrication with fusion-based processes. For such materials as borated stainless steels, Friction Freeform Fabrication can prove to be a very useful process. In this case, as material deposition takes place in solid state, the problems discussed above are not relevant.

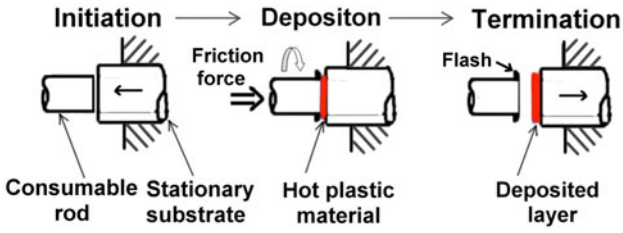

Fig. 1 Schematic illustration of friction deposition

2. Experimental Details

Friction deposition experiments were carried out on a standard direct-drive rotary friction welding machine (Make: Eta Technology, Bangalore, India) using 10 mm diameter consumable rods of borated stainless steel ASTM 304B4 Grade B (chemical composition in wt.%: Fe-0.02C-18.1Cr-12.5 Ni-1.15B-1.3Mn-0.5Si-0.02P-0.003S). The consumable rods were machined in rolling direction from 40 mm thick hot-rolled plates obtained from ArcelorMittal, France. Austenitic stainless steel (AISI 304) rods of 15 mm diameter were used as the substrate. Friction deposition was carried out using a spindle rotation speed of 800 rpm, a friction force of 8 kN, and

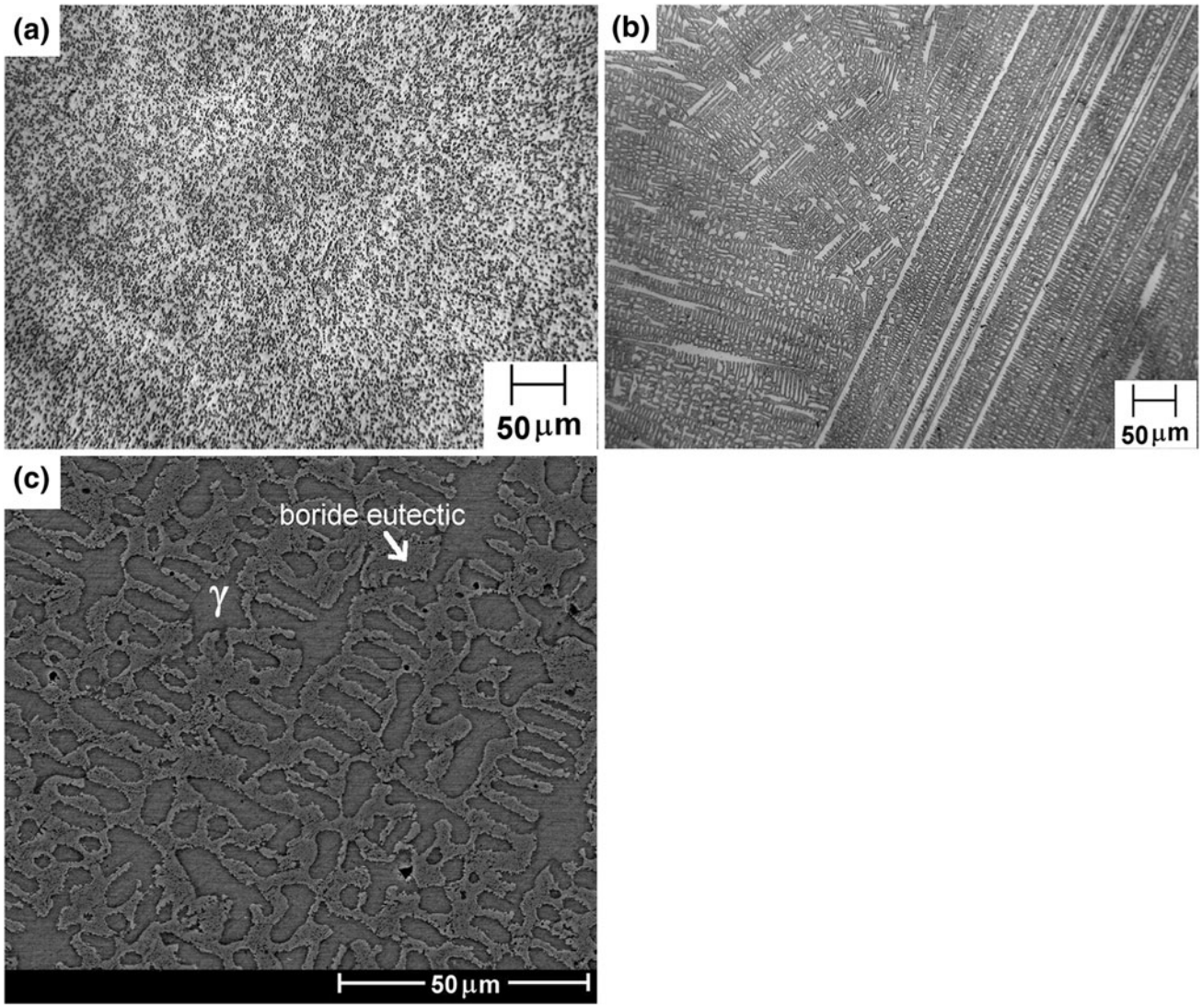

Fig. 2 Microstructures of alloy 304B7 Grade A: (a) base metal, optical; (b) weld metal, optical; (c) weld metal, SEM. Note fine, uniformly distributed boride particles in the base metal as against a continuous interdendritic network of brittle boride + austenite eutectic in the weld metal. The weld metal sample was taken from an autogenous bead-on-plate gas tungsten arc weld in 3 mm thick sheet

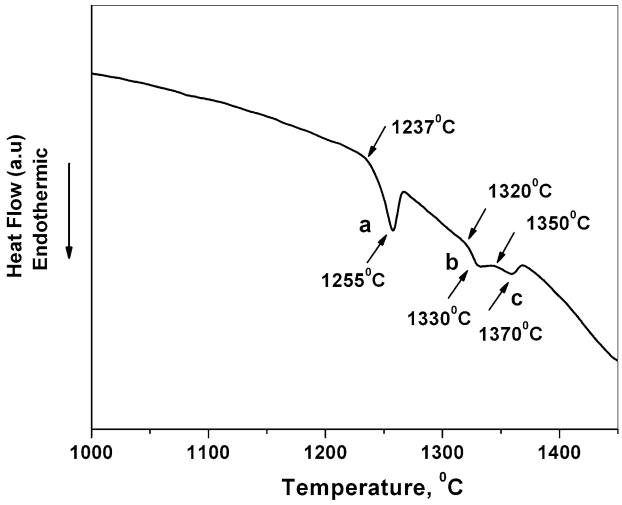

Fig. 3 DSC thermogram of alloy 304B4 Grade B (obtained on heating at a rate of 10 K/min). There are no thermal events until 1230 °C. Endotherm "a" corresponds to boride liquation. The boride-matrix eutectic reaction consumes much of the austenite. The remaining austenite melts in two stages (endotherms "b" and "c")

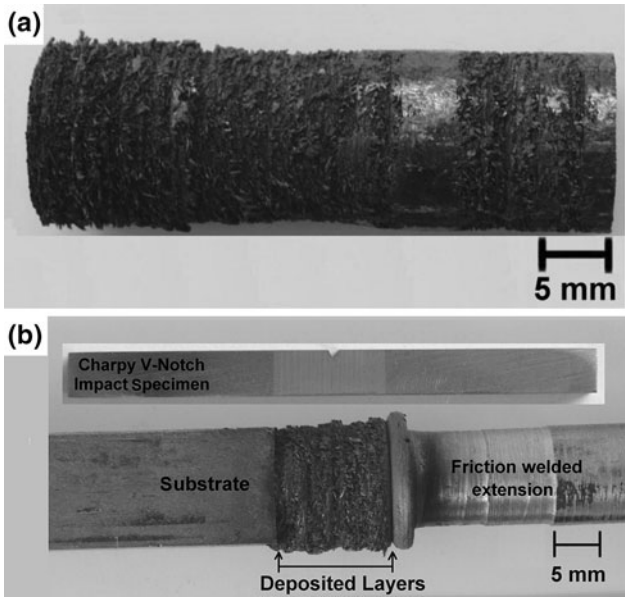

Fig. 4 Photographs of friction-deposited cylindrical samples produced for tensile (a) and impact (b) testings

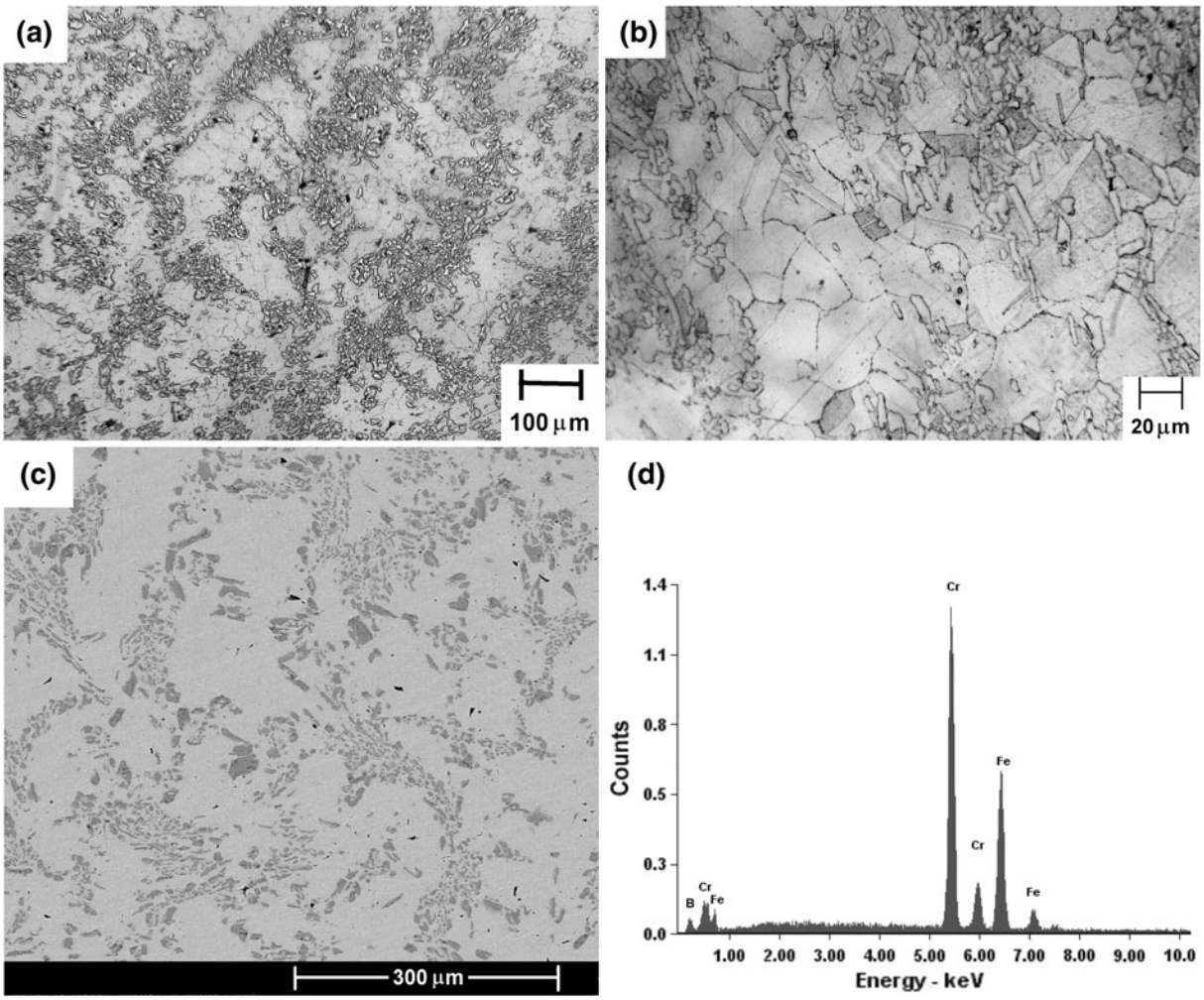

Fig. 5 Microstructures of the consumable rod: (a) and (b) optical micrographs, (c) SEM micrograph, and (d) EDS spectrum obtained on a boride particle

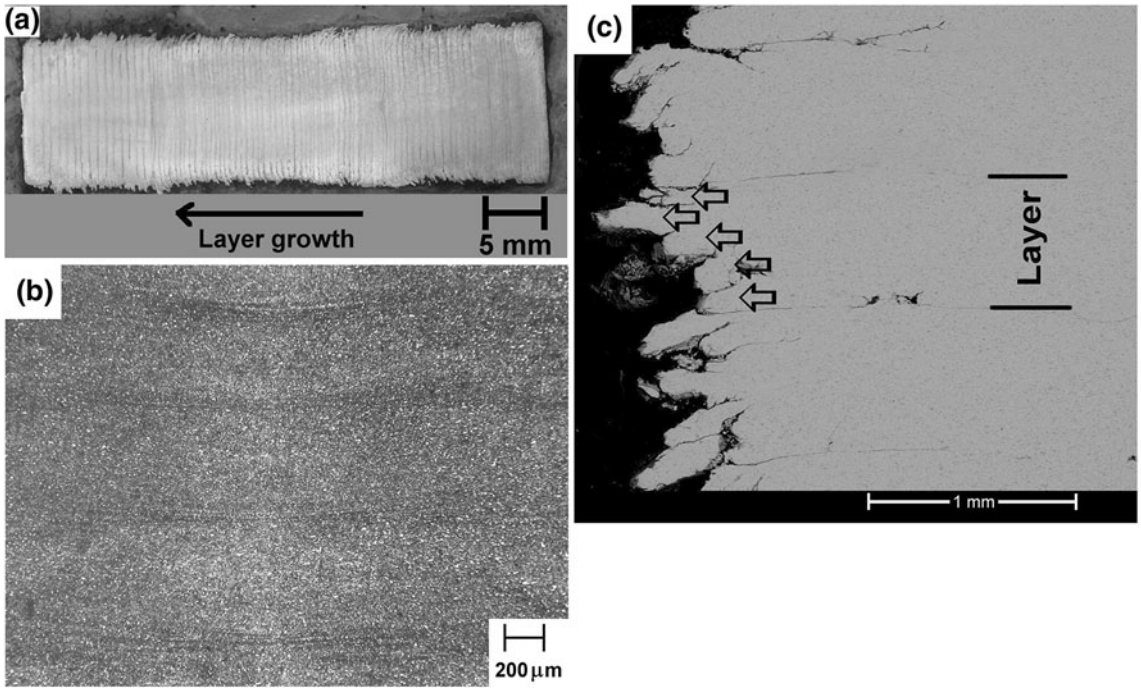

Fig. 6 (a) Macrograph of the friction deposit (longitudinal section). The sample consisted of more than 70 layers. (b) Optical micrograph of the friction deposit. (c) SEM micrograph at the edge of the friction deposit. Arrows show thin, discrete layers within a friction-deposited layer

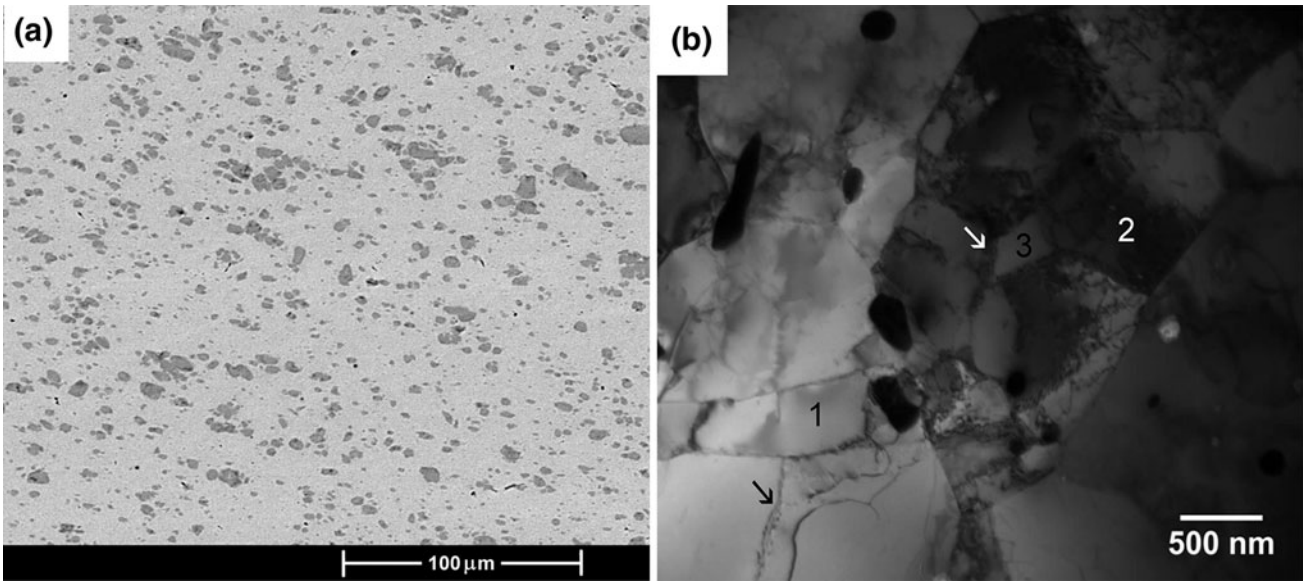

Fig. 7 SEM (a) and TEM (b) microstructures of the friction deposit. In (b), Annotations 1 and 2 show grains with low and high dislocation densities, respectively. Annotation 3 marks a cell with dense dislocation walls (white arrow). The black arrow shows a developing cell boundary. The dark particles seen in the picture are fine boride particles

a friction time of about 40 s. These parameters were arrived at based on prior experiments. A layer thickness ranging from 0.5 to 0.6 mm (after surface machining) was maintained throughout the build. After completing the build, the deposit was cut from the substrate. Figure 4(a) shows a friction-deposited cylindrical sample (40 mm height) produced in this study.

The thermal cycles involved in friction deposition were determined using a calibrated infrared camera (CEDIP JADE mercury cadmium telluride camera, Flir System, Croissy-Beaubourg, France), capable of measuring temperatures up to 1500 °C. More details on these experiments can be found elsewhere (Ref 12).

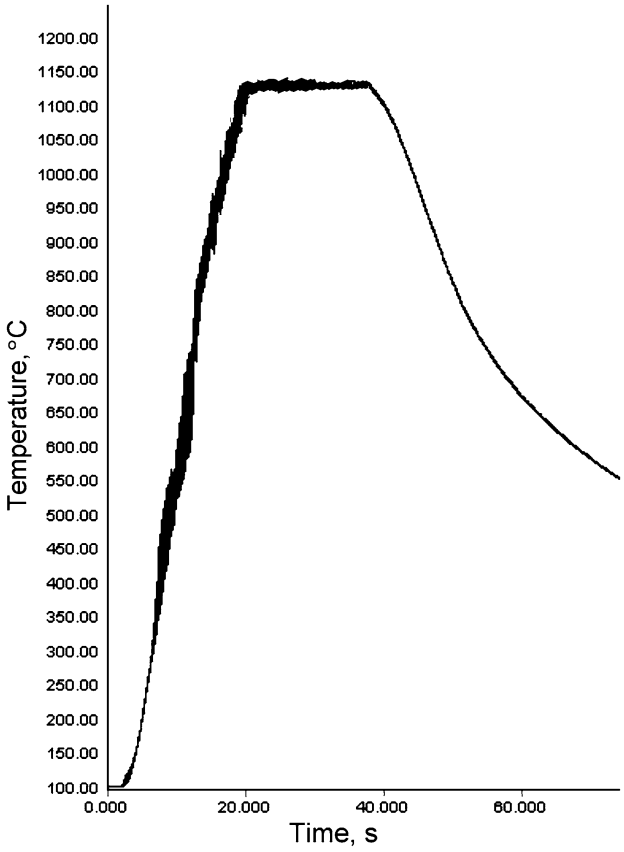

Fig. 8 Average temperature close to the rotating consumable rod/substrate interface as a function of time during friction deposition

One of the friction deposits was cut longitudinally and was prepared for microstructural examination following standard metallographic procedures. After polishing, the specimen was etched with Kalling's reagent (5 g $CuCl_2$, 100 ml HCl, and 100 ml Ethanol). Microstructural studies were performed using optical and scanning electron microscopes (SEM) in both as-polished and etched conditions. Energy dispersive spectroscopy (EDS) was used for microchemical analysis. For transmission electron microscopy (TEM), thin foil specimens were prepared using electrolytic jet polishing in 10 vol.% perchloric acid solution. Microstructural studies were also conducted on the consumable rod material for comparison.

Brinell hardness tests were conducted on friction deposits and consumable rods as per ASTM E10. Hardness measurements were carried out using a 2.5 mm diameter tungsten carbide ball indenter with a load of 187.5 kg applied for 15 s. At least, five measurements were made in both cases. Uniaxial room temperature tensile tests were conducted on standard flat sub-size specimens machined from friction deposits. The layers were oriented perpendicular to the specimen length. These specimens (2 mm thickness, 10 mm gauge length, 3 mm gauge width, 5 mm fillet radius, and 40 mm total length) conform to the requirement of ASTM E8. Tests were carried out on a universal testing machine at a crosshead speed of 1 mm/min.

For obtaining Charpy V-notch impact test specimens, friction deposits were produced in a different way. In this case, builds were made on 15 mm diameter rods of alloy 304B4. After building the deposit to a height of about 10 mm, the consumable rod was friction welded to the deposit. This was done only for the sake of convenience. Figure 4(b) shows the picture of a cylindrical sample produced in this way. Standard sub-size impact test specimens (5 mm × 5 mm × 55 mm) as per ASTM E23 were machined from these deposits. The notch was located at the center of the specimen in the friction-deposited layers (Fig. 4b). Tensile and impact tests were also conducted on identically machined specimens from the consumable rods. Three specimens were tested in all the cases. For fractographic analysis, tensile and impact fracture surfaces were examined using a SEM.

3. Results and Discussion

Figure 5(a) shows the optical microstructure of the consumable rod, consisting of austenitic matrix and boride particles. The boride particles were irregular in shape and size (ranging from 5 to 25 μm) and were not homogeneously distributed in the matrix. The average grain size of the austenitic matrix is around 40 μm (Fig. 5b). The SEM micrograph in Fig. 5(c) shows the boride particles more clearly. EDS analysis of these particles shows that they are rich in Cr and Fe (Fig. 5d). While both Fe_2B and Cr_2B phases can exist in borated stainless steels, it is difficult to identify them separately as Fe_2B can dissolve Cr and Cr_2B can dissolve Fe (Ref 13). Overall, the microstructural features seen in the consumable rod material are typical of borated stainless steels processed via ingot metallurgy route (Grade B materials). Also, a comparison of Fig. 2(a) with Fig. 5(a) clearly shows that Grade A materials are superior to Grade B materials in terms of boride shape, size, and distribution.

Figure 6(a) shows the longitudinal section of a friction deposit produced in this study. While the layer interfaces could be distinctly seen because of etch contrast, all the layers are metallurgically bonded to each other without any physical discontinuities or defects at the layer interfaces (Fig. 6b). There is, however, a small unbonded region (about 1 mm wide) in each layer at the outer periphery (Fig. 6c). This is a common feature in friction deposits due to the effect of material roll-over (Ref 7, 14). In the context of additive manufacturing, these small unbonded regions are not of serious concern as they can be subsequently machined off.

More importantly, observations at the deposit edges revealed that each friction-deposited layer consisted of several discrete layers of about 0.1 mm, shown by arrows in Fig. 6(c) (these are not revealed in the deposit microstructure away from the edges). This suggests that during friction deposition, material transfer (from the consumable rod to the substrate) occurs in discrete layers. Accordingly, the process of friction deposition can be understood as follows. As the consumable rod is rotated against the substrate, heat is generated at the rubbing interface, and the temperature at the tip of the consumable rod begins to rise. The rise in temperature of the substrate is much less because of the larger heat sink. Simultaneously, the material at the tip of the consumable rod begins to deform under the applied axial force. Frictional forces also result in removal of the surface oxide layers (they get broken into small pieces, which get distributed in the plastically deforming metallic matrix). As the process progresses, a stage is eventually reached where the mating surfaces stick to each other because of intimate nascent metal contact. After this event, continued

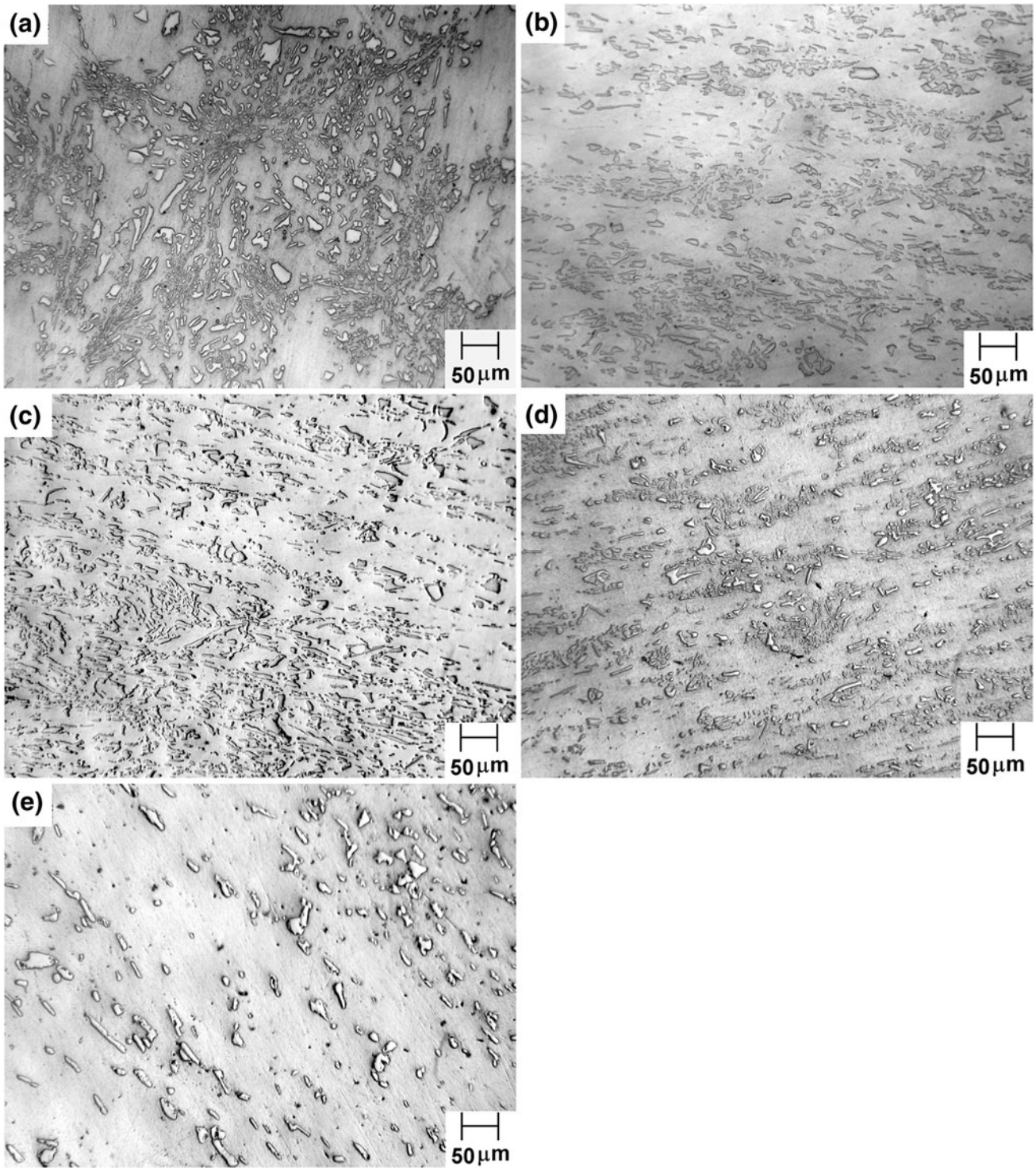

Fig. 9 Optical micrographs of alloy 304B4 Grade B in as-received and after 4 h of exposure at different temperatures: (a) As-received, (b) 1075 °C, (c) 1125 °C, (d) 1175 °C, and (e) 1225 °C. The borides show no signs of coarsening even after 4 h of exposure at temperatures as high as 1175 °C

rotation of the consumable rod results in severe torsional deformation [causing further heating due to viscous heat dissipation (Ref 15)] and shearing of the consumable rod material at a certain distance from the original rubbing interface where the material is not sufficiently hot and plastic. In this process, a discrete layer of material gets transferred from the consumable rod to the substrate and the plane of rotation shifts to the point where shear occurs. Thus, as the process continues, the stick and shear events alternate with each other, and the overall thickness of the material transferred to the substrate increases with time. When the process is finally terminated, the consumable rod separates from the deposited material at the

instantaneous rotational plane. These ideas are in line with those put forth by other investigators explaining the mechanism of material transfer in friction surfacing (Ref 16-19).

As can be seen from Fig. 6(b) and 7(a), the friction deposit consisted of finer (average size around 2 μm) and more uniformly distributed boride particles compared with the consumable rod (Fig. 5a, c). The boride microstructure of the friction deposit closely resembles that of Grade A materials (Fig. 2a). There are no perceivable changes in the deposit microstructure from layer-to-layer, suggesting that the effects of multiple thermal cycles are minimal. The grain size of the friction deposit is also extremely fine (around 1 μm), as can be seen from the TEM microstructure shown in Fig. 7(b). These observations suggest that friction deposition of alloy 304B4 Grade B involves no detrimental microstructural changes. Rather, the process benefits the microstructure of the material in many respects.

Friction deposition involves severe plastic deformation of the consumable rod material at high homologous temperatures (0.8-0.9) and high strain rates (more than 400 s^{-1}) (Ref 15, 20-22). In the current study, using infrared thermography, a peak temperature of 1130 °C was measured during friction deposition of alloy 304B4 (Fig. 8). This is much less than the eutectic melting temperature of the borides in alloy 304B4 (as per Fig. 3) and is also not high enough to cause any coarsening of the boride particles. Isothermal annealing experiments conducted in this study show that the boride particles in alloy 304B4 Grade B do not coarsen significantly even after 4 h of exposure at temperatures as high as 1175 °C (Fig. 9). The absence of any solid-state phase transformations in alloy 304B4 further simplifies the case. It should be noted that the thermal cycles involved in friction deposition are not as benign and harmless as they may appear to be from the current results on borated stainless steels. In material systems such as heat-treatable aluminium alloys, serious microstructural complications can arise during friction deposition (for example, overaging of strengthening precipitates). In such cases, it is necessary to appropriately heat treat the friction deposits to achieve satisfactory microstructures and properties.

Table 1 Mechanical test results

Property	Alloy 304B4 Grade B		
	Specified (ASTM 887)	Obtained	Friction deposit
Tensile			
0.2% yield strength, MPa	205	250	330
Ultimate tensile strength, MPa	515	620	700
Elongation, %	16	20	28
Charpy V-notch energy, J	…	5	11
Hardness, HBW	217	220	250

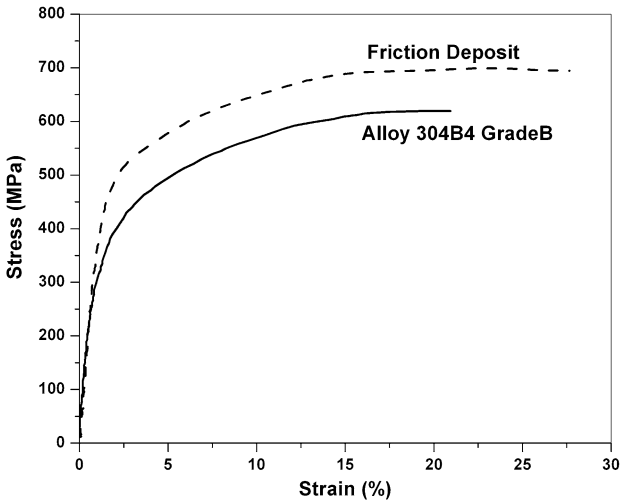

Fig. 10 Typical tensile stress-strain plots of alloy 304B4 Grade B and friction deposit

During friction deposition, because of the severe plastic deformation involved in the process, any non-deformable particles in the consumable rod material, such as the borides in the present case, can be expected to break into smaller pieces and be distributed in the matrix material more or less uniformly. Such phenomena involving fragmentation and redistribution of the hard second phases have been previously reported in friction surfacing (Ref 12) and friction stir welding/processing (Ref 23) literature. These phenomena are responsible for the finer and more uniformly distributed boride particles seen in friction deposits compared with the consumable rods. Further, because of the severe plastic deformation at high temperatures and strain rates, the consumable rod material can undergo a variety of hot restoration processes during friction deposition. In general, discontinuous dynamic recrystallization is the most important hot restoration mechanism in low stacking fault energy materials such as austenitic stainless steels (Ref 24). In the current study, as can be seen in Fig. 7(b), the friction deposit showed diverse microstructural features such as developing cell boundaries, cells with dense dislocation walls, and fully recrystallized grains, suggesting that the material had undergone discontinuous dynamic recrystallization during friction deposition. Similar findings have been reported in friction surfaced austenitic stainless steel coatings (Ref 20, 22). It should be noted that such a fine grain size is difficult to achieve in borated stainless steels with conventional thermo-mechanical processing.

The mechanical properties of friction deposits as well as those of standard wrought processed alloy 304B4 Grade B material (i.e., consumable rods used for friction deposition) are presented in Table 1. The specified minimum properties for alloy 304B4 Grade B are also included in the table. Figure 10 shows the typical tensile stress-strain plots of the two materials. As can be seen, friction deposits not only meet the specification requirements, but are also significantly harder, stronger, and tougher compared to their wrought counterparts. Examination of the tensile and impact fracture surfaces of both the materials revealed ductile, dimpled rupture features with occasional boride decohesion and cracking (Fig. 11), as observed in earlier investigations (Ref 9, 13). The microvoids were, however, finer and more equiaxed in friction deposits because of their refined boride microstructure.

Overall, it is seen that Friction Freeform Fabrication works very well for part fabrication in borated stainless steel 304B4. Being a solid-state process, it overcomes the major problems associated with fusion deposition of this material (solidification cracking, liquation cracking, and formation of a continuous network of brittle boride eutectic). Parts can be produced using inexpensive Grade B consumable rod materials, as during the process of friction deposition, the microstructure of the material is beneficially influenced in many ways, leading to fine and

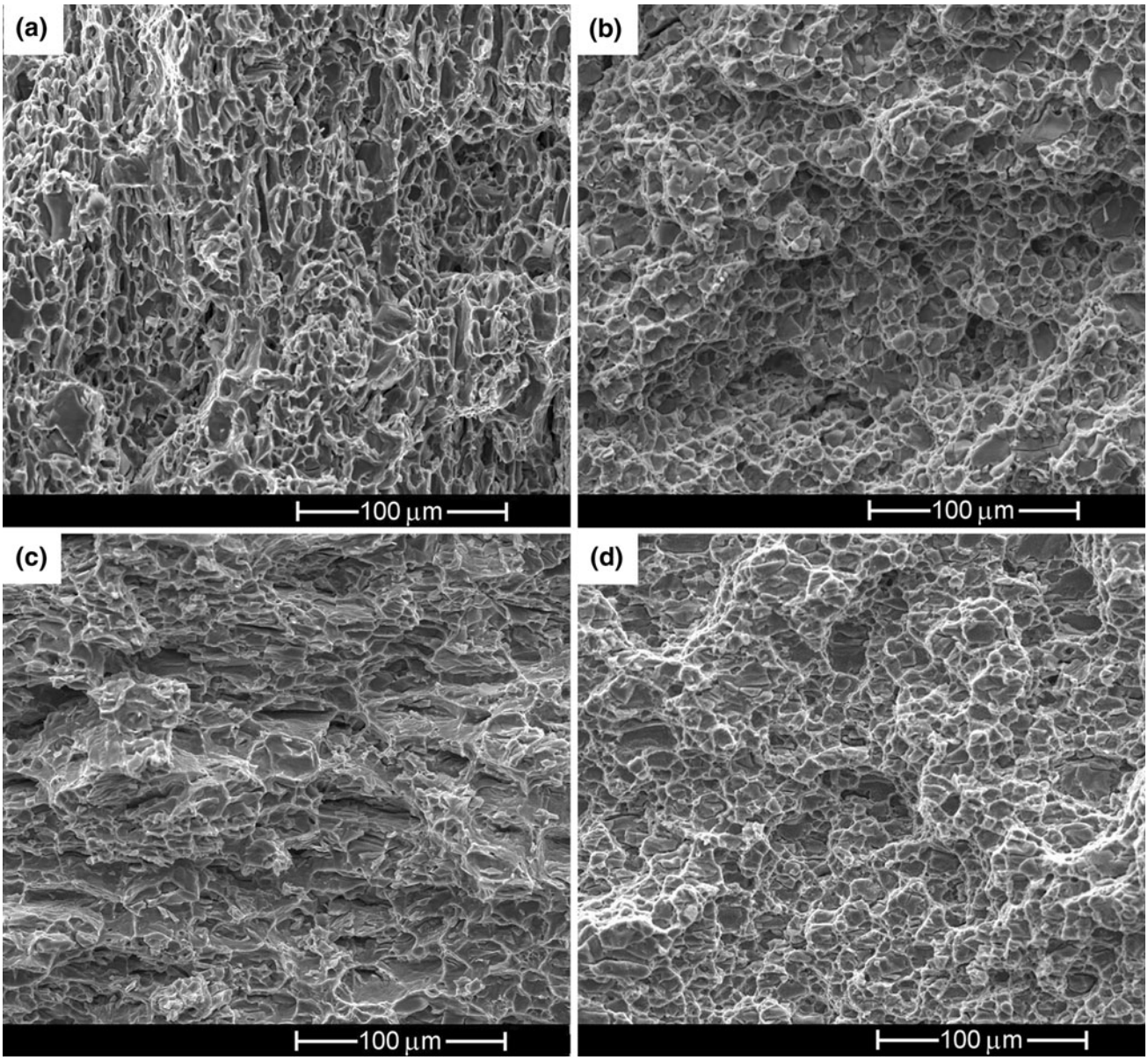

Fig. 11 Fracture surfaces: (a) consumable rod, tensile; (b) friction deposit, tensile; (c) consumable rod, impact; and (d) friction deposit, impact. Note finer and more equiaxed dimples in friction deposits

uniformly distributed boride particles and very fine matrix grain size. As a result, parts produced using Friction Freeform Fabrication in alloy 304B4 show superior tensile, hardness, and impact properties to standard wrought-processed alloy 304B4 Grade B. The authors believe that Friction Freeform Fabrication can help borated stainless steels in being advantageously utilized in place of conventional austenitic stainless steels in a variety of engineering applications such as injection mounding dies and tooling.

4. Conclusions

In the current study, friction deposition experiments were conducted using borated stainless steel ASTM 304B4 Grade B consumable rods. Microstructural and mechanical properties of the friction deposits were compared to those of the consumable rods used for producing them. The following conclusions can be drawn from the current study:

- Borated stainless steel 304B4 can be readily friction deposited with excellent layer-to-layer bonding. Cylindrical samples of 40 mm height and 10 mm diameter, consisting of more than 70 layers, were successfully produced.
- Thermal cycles involved in friction deposition have no detrimental effect on alloy 304B4 microstructure. In fact, the process significantly improves the microstructure of the material in terms of matrix grain size as well as boride size, shape, and distribution.
- Friction deposits in alloy 304B4 show superior hardness, tensile, and impact properties compared with standard wrought-processed alloy 304B4 Grade B.
- Friction Freeform Fabrication is well suited for additive

part fabrication in such materials as borated stainless steels that are difficult to fusion deposit.

References

1. K.N. Amato, S.M. Gaytan, L.E. Murr, E. Martinez, P.W. Shindo, J. Hernandez, S. Collins, and F. Medina, Microstructures and Mechanical Behavior of Inconel 718 Fabricated by Selective Laser Melting, *Acta Mater.*, 2012, **60**(5), p 2229–2239
2. O.L.A. Harrysson, O. Cansizoglu, D.J.M. Little, D.R. Cormier, and H.A. West, II, Direct Metal Fabrication of Titanium Implants with Tailored Materials and Mechanical Properties Using Electron Beam Melting Technology, *Mater. Sci. Eng. C*, 2008, **28**(3), p 366–373
3. I. Palcic, M. Balazic, M. Milfelner, and B. Buchmeister, Potential of Laser Engineered Net Shaping (LENS) Technology, *Mater. Manuf. Process.*, 2009, **24**(7-8), p 750–753
4. Z.L. Lu, A.F. Zhang, Z.Q. Tong, X.H. Yang, D.C. Li, and B.H. Lu, Fabricating the Steam Turbine Blade by Direct Laser Forming, *Mater. Manuf. Process.*, 2011, **26**(7), p 879–885
5. J.J.S. Dilip, G.D. Janaki Ram, and B.E. Stucker, Additive Manufacturing with Friction Welding and Friction Deposition Processes, *Int. J. Rapid Manuf.*, 2012, **3**(1), p 56–69
6. J.J.S. Dilip, S. Babu, S. Varadha Rajan, K.H. Rafi, G.D. Janaki Ram, and B.E. Stucker, Use of Friction Surfacing for Additive Manufacturing, *Mater. Manuf. Process.*, 2013, **28**(2), p 189–194
7. S. Grainger and J. Blunt, *Engineering Coatings: Design and Application*, 2nd ed., Abington Publishing, Cambridge, 1998
8. ASTM Standard A887-89 (2009), "Standard Specification for Borated Stainless Steel Plate, Sheet, and Strip for Nuclear Application," ASM International, West Conshohocken, PA, USA
9. C.V. Robino and M.J. Cieslak, Fusion Welding of Borated Stainless Steels, Report # SAND-93-3981, Sandia National Laboratories, Albuquerque, USA, 1994, doi:10.2172/10183280
10. C.V. Robino and M.J. Cieslak, Fusion Welding of a Modern Borated Stainless Steel, *Weld. J.*, 1997, **76**(1), p 11–23
11. T.D. Park, K.K. Baek, and D.S. Kim, PWHT Effect on the Mechanical Properties of Borated Stainless Steel GTA Weldments for Nuclear Shield, *Met. Mater.*, 1997, **3**(1), p 46–50
12. R. Puli and G.D. Janaki Ram, Microstructures and Properties of Friction Surfaced Coatings in AISI, 440C Martensitic Stainless Steel, *Surf. Coat. Technol.*, 2012, **207**, p 310–318
13. C.V. Robino and M.J. Cieslak, High Temperature Metallurgy of Advanced Borated Stainless Steel, *Metall. Mater. Trans. A*, 1995, **26**, p 1673–1685
14. H.K. Rafi, G.D. Janki Ram, G. Phanikumar, and K. Prasad Rao, Microstructure and Properties of Friction Surfaced Stainless Steel and Tool Steel Coatings, *Mater. Sci. Forum*, 2010, **638-642**, p 864–869
15. H.K. Rafi, K. Balasubramaniam, G. Phanikumar, and K. Prasad Rao, Thermal Profiling Using Infrared Thermography in Friction Surfacing, *Metall. Mater. Trans. A*, 2011, **42**, p 3425–3429
16. K. Fukakusa, On the Characteristics of the Rotational Contact Plane—A Fundamental Study of Friction Surfacing, *Weld. Int.*, 1996, **10**(7), p 524–529
17. G.M. Bedford, V.I. Vitanov, and I.I. Voutchkov, On the Thermo-Mechanical Events During Friction Surfacing of High Speed Steels, *Surf. Coat. Technol.*, 2001, **141**, p 34–39
18. X.M. Liu, Z.D. Zou, Y.H. Zhang, S.Y. Qu, and X.H. Wang, Transferring Mechanism of the Coating Rod in Friction Surfacing, *Surf. Coat. Technol.*, 2008, **202**, p 1889–1894
19. H.K. Rafi, G. Phanikumar, and K. Prasad Rao, Material Flow Visualization During Friction Surfacing, *Metall. Mater. Trans. A*, 2011, **42**, p 937–939
20. R. Puli and G.D. Janaki Ram, Dynamic Recrystallization in Friction Surfaced Austenitic Stainless Steel Coatings, *Mater. Charact.*, 2012, **74**, p 49–54
21. K. Prasad Rao, A. Veera Sreenu, H.K. Rafi, M.N. Libin, and K. Balasubramanian, Tool Steel and Copper Coatings by Friction Surfacing—A Thermography Study, *J. Mater. Process. Technol.*, 2012, **212**, p 402–407
22. H.K. Rafi, N. Kishore Babu, G. Phanikumar, and K. Prasad Rao, Microstructural Evolution During Friction Surfacing of Austenitic Stainless Steel AISI, 304 on Low Carbon Steel, *Metall. Mater. Trans. A*, 2013, **44**, p 345–350
23. R.S. Mishra and Z.Y. Ma, Friction Stir Welding and Processing, *Mater. Sci. Eng.*, 2005, **50**(1-2), p 1–78
24. F.J. Humphreys and M. Hatherly, *Recrystallization and Related Annealing Phenomena*, 2nd ed., Elsevier, Oxford, UK, 2004